EU contract number RII3-CT-2003-506395   CARE-Report-2007-031-PHIN

Final Report on 100 MeV Laser Driven Plasma Source R&D

V. Malka, J. Faure, Y. Glinec, A. Lifschitz, C. Réchatin

Laboratoire d'Optique Appliquée – ENSTA, UMR7639, CNRS, Ecole Polytechnique, 91761 Palaiseau, France

Abstract

We report the results obtained within the CARE/PHIN related to activity done at LOA in the SPL group on laser plasma accelerators.

I. Introduction.

Plasma-based accelerators have been proposed for the next generation of compact accelerators because of the huge electric fields they can support. However, it has been difficult to use them efficiently for applications because they produce poor quality particle beams with large energy spreads. By focusing light pulses containing a few joules of energy in a few tens of femtoseconds onto gas jets, extremely large electric fields can be generated, reaching the teravolts per metre level. As a result, the length over which electrons extracted from the target can be accelerated to hundreds of MeV is reduced to a few millimetres. The reduction of the size and the cost of laser-plasma accelerators is a promising consequence, but these electron beams also reveal original properties, which make them a wonderful tool for science. By adjusting the interaction parameters, the electron energy distribution can be tuned from a maxwellian-like distribution to a quasi-monoenergetic one. The new properties of these laser-based particle beams are well suited to many applications in different fields, including medicine (radiotherapy), chemistry (ultrafast radiolysis), material science (non-destructive material inspection using radiography) and, of course, for accelerator physics. The purpose of our contribution in the project was the development of compact single shot electron spectrometers in order to optimise the coupling of the laser beam into the electron beam and especially to control the electron distribution energy. This has allow us to understand specific feature of the interaction, to demonstrated new scheme of injection (bubble and colliding), and to explore new applications. We report here the work realized thanks to the support of CARE.

II. Towards a monoenergetic electron beam: The bubble regime.

Electron spectra.

For entering the bubble regime (1,2), the pulse duration should be shorter than the plasma period. For 30 fs pulses, this can be done by lowering the plasma density below 10^{19} cm^{-3}. Furthermore, the interaction length should be long enough for the laser pulse to evolve (self-focus and self-compress) and so that electrons can be trapped and accelerated on a long enough distance (i.e. the dephasing length). A simple solution to this problem is to simply extend the Rayleigh length to millimetre scale by focusing the beam with long focal length optics. By focusing the beam with smaller aperture optics, it was possible, even with 10 times lower laser intensity, to produce higher electron energy gain. By matching the propagation length (here the Rayleigh length) with the dephasing length (length over which electron are accelerated), this process has been optimized - it has been possible to generate a very high quality electron beam (3-5) with a single laser beam at moderate energy (~ 1J). Experiments have been done at LOA facility the "salle jaune laser" with the compact 10 Hz, powerful laser system. The laser is based on a classical Chirp Pulse Amplification (CPA) (6). Routinely, the laser delivers an output on-target energy of 1.2 J with duration of 30 fs, which produces a peak power of 40 TW. The use of gas jets to generate a suitable density interaction medium is important, even crucial for many laser plasma interactions experiments. The control, the stability and the robustness of the targets, which will be irradiated to produce plasmas, are the main criteria for those experiments. Gas targets will be a key issue of the applicability of laser plasma accelerators concept in both uniform-plasma (3,5) or plasma-channel approaches (4) since they offer the possibility of high repetition-rate, long-lifetime systems. Accurate control of the target parameters are also important for the understanding of the fundamental processes involved during the interaction since one needs to know with accuracy the plasma parameters. Controlling the density value and the density profile will also permit an accurate

benchmarking of simulation codes. Gas jet targets are, for these reasons, highly suitable for laser-plasma accelerator targets. Special efforts have been made in order to optimize the gas flow for laser plasma experiments (7). After compression the laser propagates under vacuum into the 1 m diameter interaction chamber. The beam is focused using a 1 m focal length off axis parabolic mirror, which corresponds to f/18 laser aperture, giving a focal spot with radius at full width half maximum of 18 μm, and producing a laser intensity of $I=3.2\times10^{18}$ W/cm^2. This choice of small aperture gives a long Rayleigh length of about 1.3 mm range of interest for higher energy gain as mentioned above. The corresponding normalized vector potential is therefore $a_0=eA/(mc^2)=1.3$ (A is the laser vector potential, e and m are respectively the charge and mass of the electron). At this intensity, the helium gas jet is fully ionised early in the interaction. Since the electron density value is not high, ionisation induced refraction does not seem to play an important role. The focal position and its value with respect to the sharp gas jet gradient have been measured and varied in order to optimise the electron beam parameter. This optimum position is found when focusing the laser beam on the edge of the plateau of the gas jet. Alignments of the laser with respect to the nozzle are performed using two imaging systems (side and top view images). Instead of measuring the electron energy spectra by using a few diodes, we chose for a new method based on the use of a compact spectrometer developed for this purpose within the CARE/PHIN contract. Doing so, we were able to measure, in a single shot, the whole spectra is imaged on a LANEX screen and to record its image on a 16 bit Charged Coupled Device (CCD) camera. Since we do not use a collimator, the vertical direction on the LANEX screen corresponds to the angular aperture of the electron beam. The LANEX screen was protected by a 100 μm thick Aluminium foil in order to avoid direct exposure to the laser light. For deconvolution of the images obtained with the LANEX screen, electron deviation in the magnetic field has been considered as well as the electron stopping power inside the LANEX screen. The resolution is limited by the electron beam aperture and by the dispersing power of the magnet. This gives a resolution of respectively 32 MeV and 12 MeV for 170 MeV and 100 MeV energies. Above 200 MeV, the resolution quickly degrades. Spatial electron beam distribution has been also measured by removing the magnet. The charge of the electron beam was measured using an integrating current transformer placed 30 cm behind the LANEX screen and the number of count on the camera. The complete design and calibration of the whole spectrometer and LANEX screen has been done within the CARE project (8).
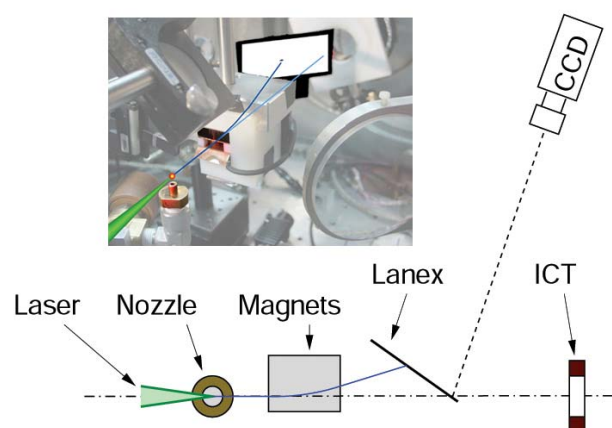

Figure 1 : Experimental set-up

Fig.2 shows a picture of the electron beam when no magnetic field is applied. By decreasing the electron density of the plasma medium, the spatial distribution of the electron beam has been dramatically improved. In the lower density cases ($<1.0\times10^{19}$cm^{-3}), the electron beam is very well collimated (below 10 mrad divergence at FWHM). One can explain this low divergence using several arguments: (i) electrons are accelerated in the plasma bubble but

they stay behind the laser pulse and do not interact with its defocusing transverse field, (ii) when electrons exit the plasma, their energy is very high and therefore, the effect of space charge is greatly diminished.
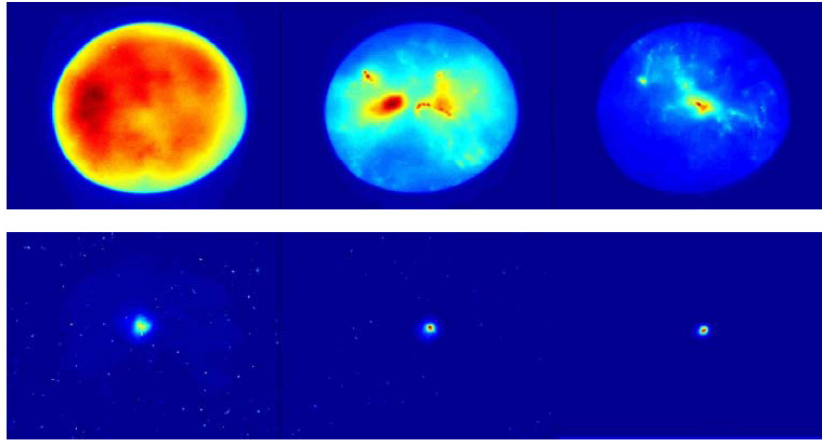

Figure 2 : Electron beam profile for plasma densities

Fig. 3 shows the raw images obtained on the LANEX screen for different densities. The picture illustrates the transition from a Maxwellian-like spectrum with an emerging monoenergetic component to a spectrum containing a very well defined monoenergetic component. This transition occurs for densities around $1.0 \times 10^{19} cm^{-3}$. The best coupling for obtaining a high charge and a quasi-monoenergetic electron beam is at $n_e = 6 \times 10^{18} cm^{-3}$. For this density, the image shows a narrow peak around 170 MeV, indicating efficient monoenergetic acceleration with a 24% energy spread (corresponding to the spectrometer resolution). The electron beam energy was estimated to be close to 100 mJ, which correspond to almost 10% of the laser energy. At lower density, the peak energy is at approximately the same position whereas the number of electrons is reduced by a factor of 10. At higher density, the peak component is still visible but starts to merge with the maxwellian body of the distribution. 3D PIC simulations done by A. Pukhov confirm this evolution and are in good agreement with the experimental data.

Bunch duration.

Production of ultrashort electron bunches is of particular interest for a large range of applications where time resolution is required. In principle, relativistic laser-plasma interaction in the bubble regime is able to produce such sub-100 fs bunches. Simulations have indicated that bunches as short as 10–30 fs can be produced in the bubble regime. We have used transition radiation of the electron bunch which is emitted by a particle going through an interface to evidence the short duration of the electron bunch.
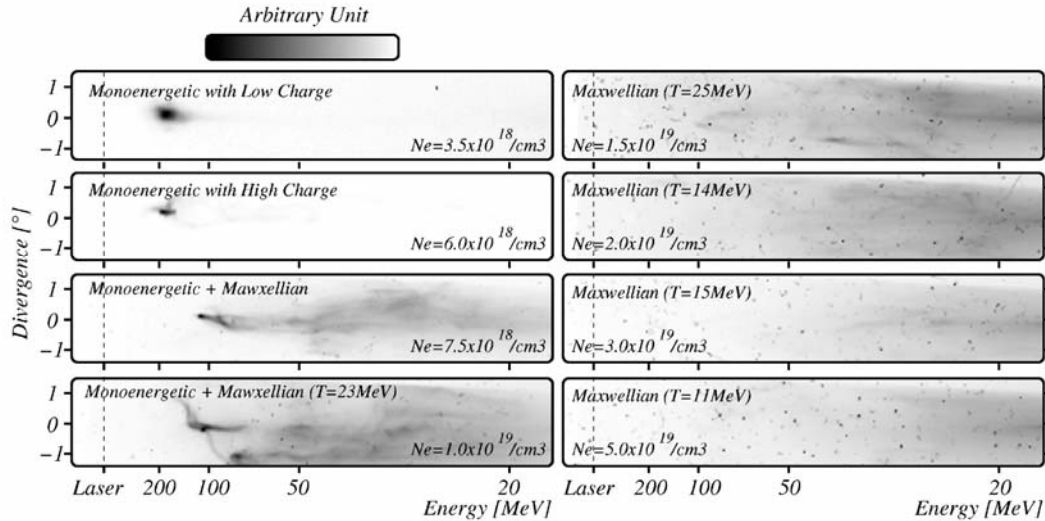
Figure 3: electron spectra for different plasma density

Measuring the spectrum gives information on the bunch shape and consequently on the bunch duration. For instance, by measuring coherent transition radiation at 10 μm, one can infer that the electron bunch has 30–50 fs structures in its temporal profile. Transition radiation depends on many different factors and it is only useful as a diagnostic if all of the crucial parameters are measured precisely. The following quantities should be known in order to model the problem properly (the geometry of the problem: collection angles, size of the radiator, type of radiator; the electron beam transverse distribution; and the energy distribution of the electron beam). If these quantities are measured, then the only unknown of the problem is the electron bunch temporal shape. Thus, by fitting the model to the experimental results, one can retrieve information on the bunch shape (9). In what follows, we present spectral measurements of coherent transition radiation in the 8–10 μm range. The results suggest sub-50 fs structures in the electron bunch. The electron beam is generated during the interaction of the laser with the gas jet. A 100 μm thick aluminum foil was placed 3 mm behind the gas jet. The foil acted as a radiator for transition radiation when the electron beam passed through it. It also blocked the laser light and prevented it from propagating to the detectors. The electron beam angular and energy distribution were measured on each shot with the electron spectrometer described earlier. The electron beam divergence was obtained by turning off the magnet on the spectrometer. The beam had a near-cylindrical symmetry and had a typical divergence of 8±1.5 mrad FWHM. The electron spectrum shows quasi-monoenergetic spikes and electron energies extending up to about 200 MeV. The position of the spikes varied from shot to shot but the overall charge in the 20–200 MeV range stayed close to about 1 nC. Note that, knowing the angular distribution of the beam and assuming a ballistic propagation, one can compute its transverse distribution at the radiator location. Transition radiation of the electron beam passing through the foil produced infrared radiation which was detected using a nitrogen-cooled HgCdTe infrared absolute calibrated detector. Various filters were added to the beam path in order to cut all laser light. Similarly, the IR radiation was coupled out of the vacuum chamber using a 3 mm thick, high resistivity silicon window. A strong optical signal at 8–10 μm was detected when the interaction produced a high energy electron beam. Figure 4 shows the correlation between the transition radiation signal and the number of high energy electrons when various parameters of the interaction were changed. The electron beam can be optimized for highest electron energy and highest

spatial quality by adjusting the gas jet position, the laser pulse duration, and the electron plasma density.

The black diamonds in Fig. 4 represent the number of electrons above 50 MeV as a function of plasma density. As expected, the signal is the largest when the plasma density is $n_e=5\times10^{18}$ cm^{-3}, for which the ratio τ_c/λ_p=0.7<1. The empty circles represent the IR signal level, which is very well correlated to the high energy electron signal. Figure 4 shows the correlation between the amount of high energy electrons and IR signal when the position of the gas jet is moved. The highest signal is obtained for the position 1.5 mm, for which the laser pulse is focused at the edge of the nozzle. Taking into account the transmission of the filters as well as the calibration of the detector, one can compute that the energy produced by transition radiation was $dW/d\lambda \approx (6.5\pm2) \times10^{-10}$ J/μm in the 8–10 μm range. The measured signal is more than three orders of magnitude higher, proving that it is at least partially coherent. In the next section, we will see how this coherent transition radiation signal allows us to retrieve temporal information regarding the electron bunch. The fact that the transition radiation signal is coherent or partially coherent in the 8–10 μm range implies that the electron bunch has temporal structures in the 30 fs range.
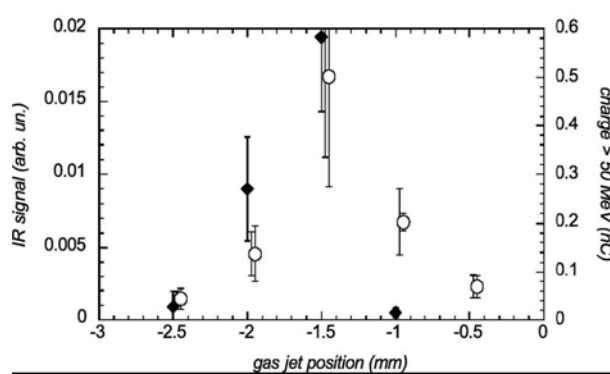

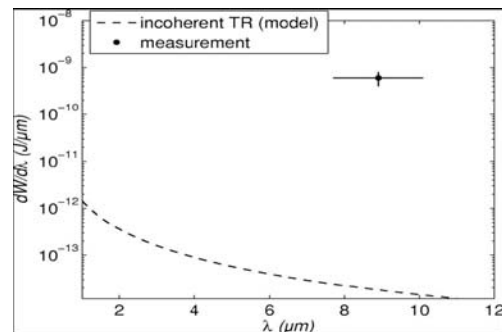Figure 4 : variation of IR and charge signals with plasma density

FIG. 5 Comparison between the signal level modelled using incoherent transition radiation (dashed line) and the measurement (full circle).

FIG. 5 shows the comparison between the signal level modelled using incoherent transition radiation (dashed line) and the measurement (full circle). The horizontal error bar indicates the wavelength range of the detection. The vertical error bar represents shot to shot fluctuations over 5 shots.

Fine temporal structure

Here, we focus on shorter wavelengths corresponding to the inner structure of the electron beam. We have used the optical transition radiation (OTR) radiation emitted by the electron beam at an interface in the visible range in order to infer the temporal fine structure of the electron beam (10). First, we show that the radiation intensity measured drops dramatically as the distance to the radiator increases, showing the coherence properties of the emission. A simultaneous measurement of the radiation spectrum at different distances reveals peaks and rapid spectral modulations, showing structures of the electron beam accelerated using a laser-plasma accelerator. An electron beam from a particle-in-cell (PIC) simulation is used to compute the OTR radiation, which successfully reproduces spectral peaks and confirms the interpretation proposed.

First, here are some evidences of the coherent nature of the OTR radiation. The integrated number of counts of the OTR images on the CCD camera have been converted into emitted energy using the absolute calibration of the detection system. Fig. 6 shows the OTR energy emitted in the range 400-1000 nm for different positions of the radiator (1.5 mm, 30 mm and 140 mm). The closer the radiator, the more intense the radiation. It's absolute value, much greater than the incoherent one, and its variation with the distance indicate the coherent nature of the radiation. Now, the radiator is placed at 30 mm from the interaction point. Fig. 7 and Fig. 8 show respectively the measured and calculated OTR spectra. The peak location at 600 nm (and not at 800 nm) is due to the interaction of electrons with the laser. Due to relativistic self-phase modulation the original laser wavelength has been blue shift during its propagation in the plasma. In our usual experimental conditions, the laser pulse is shorter than the plasma period.
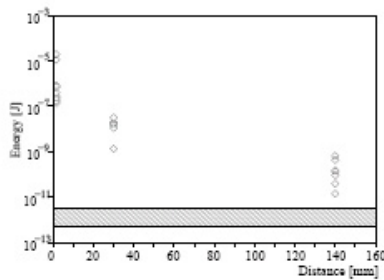
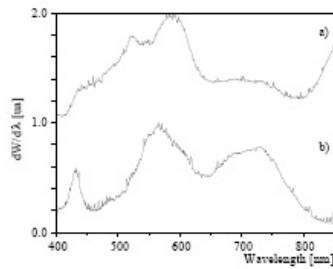*Figure 6: OTR energy for different positions of the radiator*

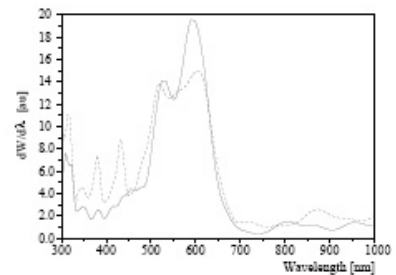*Figure 7: Measured OTR spectra for two iris diameters*

Figure 8: calculated OTR spectra using angular (dash line) and spatial (solid line) distribution.

At 1.5 mm, this technique is used to measure the delay between two bunches from the spectral modulations which results from the interference of two electron pulses separated by a delay τ. From the period of the modulations in the range 500-600 nm, one obtains a delay τ = 74 fs. The linear plasma period τ = 50 fs is slightly lower than the observed delay. But in such non-linear interaction, the plasma period might be longer than the linear case due to (i) the relativistic factor of the electrons or (ii) the beam loading (saturation of charge). The main features of the observed spectrum in Fig. 9a) are reproduced in Fig. 9b) using the temporal profile shown in the inset. The first pulse is modulated at 550 nm by the laser pulse in order to produce a peak in the radiation spectrum. The second bunch delayed by 75 fs, is not under the influence of the laser and creates a broadband OTR spectrum over the optical wavelengths which interfere with the peaked spectrum. There exist various realistic temporal profiles that allow to reproduce the observed modulations. Here, it is assumed that both electron bunches have the same electron spectrum corresponding to a measured one. The first and second bunches respectively contains 70 % and 30 % of the charge and have a duration of 10 fs and 3 fs (FWHM).
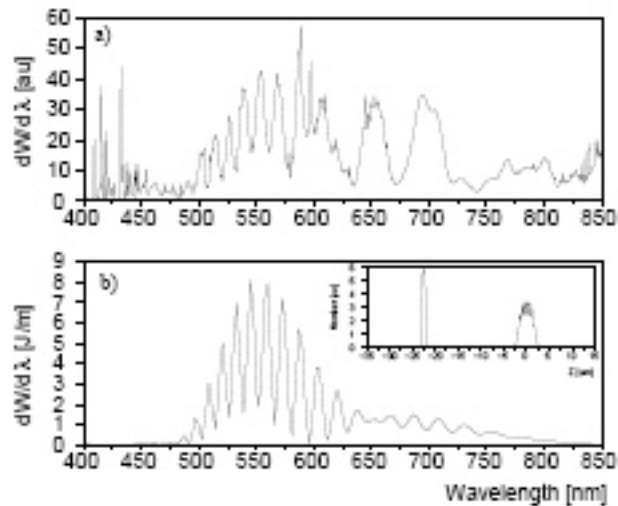
FIG. 9: (a) OTR spectrum with high frequency modulations in the range 500-600 nm. The very-high frequency signal below 450 nm contains only noise from X-rays directly detected by the CCD camera. The half-angle of collection is 70 mrad. (b) Example of OTR spectrum computed using two electron bunches, as shown in the inset.

III. Towards a monoenergetic, stable and tuneable electron beam : The colliding regime.

The second approach to generated quasi monoenergetic electron beam is based on the use of several laser pulses[11]. In its simplest form, the scheme uses two counter-propagating ultra-short pulses with the same wavelength and polarisation. The first laser pulse, the "pump" pulse, creates a wakefield whereas the second laser, the "injection" pulse is only used for injecting electrons. The laser pulses collide in the plasma and their interference creates an electromagnetic beatwave pattern which pre-accelerates some electrons. A fraction of these has enough energy to be trapped in the wakefield driven by the pump pulse and further accelerated to relativistic energies. This scheme offers more flexibility: experiments have shown that the electron beam energy can be tuned continuously from 10 to 250 MeV[12]. On Figure 10 we show the evolution of the electron beam peak energy and its energy spread versus the injection position z_{inj}, e.g. the position at which the two laser pulses collide.

The electron beam has a quasi-monoenergetic distribution with energy spread in the 5-10 % range, charges in the 10-100 pC range and its parameters are stable within 5-10%. This approach is promising for the control of the electron beam parameters, and might allow to change both the charge and the energy spread. For instance, increasing the beam energy to the GeV level should decrease the relative energy spread to the 1 % level. Lower energy beams with 1% relative energy spread could be obtained with shorter laser pulses. The electron bunch duration has never been measured experimentally with sufficient resolution but there are preliminary evidences that it might be shorter than 10 fs[13].
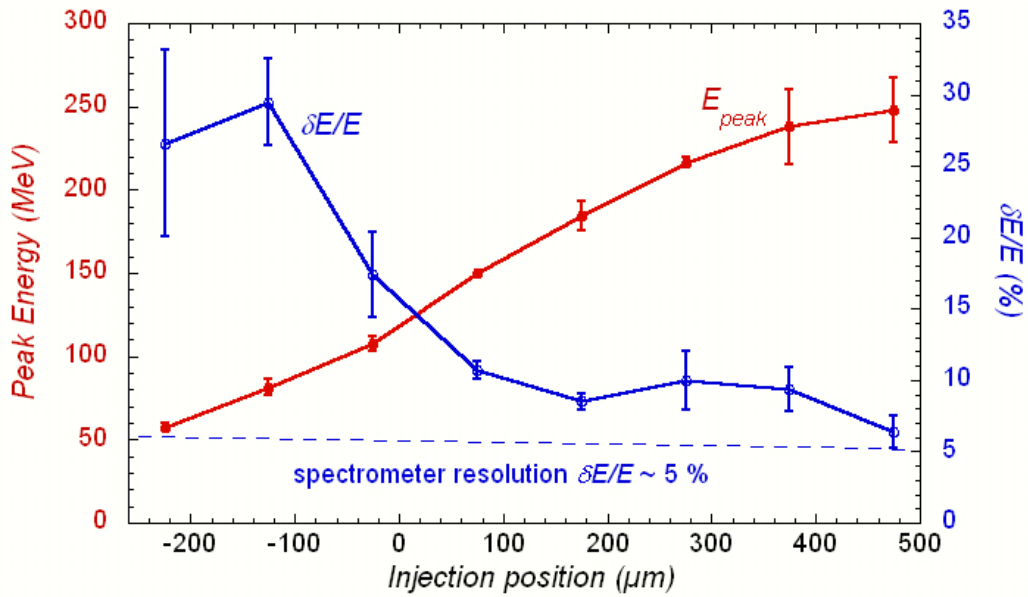
Figure 10: A graph showing the evolution of the electron beam peak energy (red curve and left vertical axis) and its energy spread (blue curve and right vertical axis) versus the injection position z_{inj}, e.g. the position at which the two laser pulses collide. Each point is an average of 3-5 shots and the error bars correspond to the standard deviation. The position $z_{inj} = 0$ corresponds to injection at the middle of the gas jet, whereas $z_{inj} = 500$ μm corresponds to early injection close to the entrance of the gas jet.

IV. Applications

Applications to radiotherapy

We show in figure 11 the dose deposition for different particles. The difference between VHE and low electron energy or photon indicates that (i) the dose deposited by electrons at a give depth is much higher than in the shorter depth than for low electron energy and photon, and (ii) than the dose deposition is still efficient after few tens of centimetres. Reducing the dose deposition before the tumour will enhance the quality of treatment and having dose deposition after tens of centimetres could be benefit to cure efficiently cancer of obese persons.
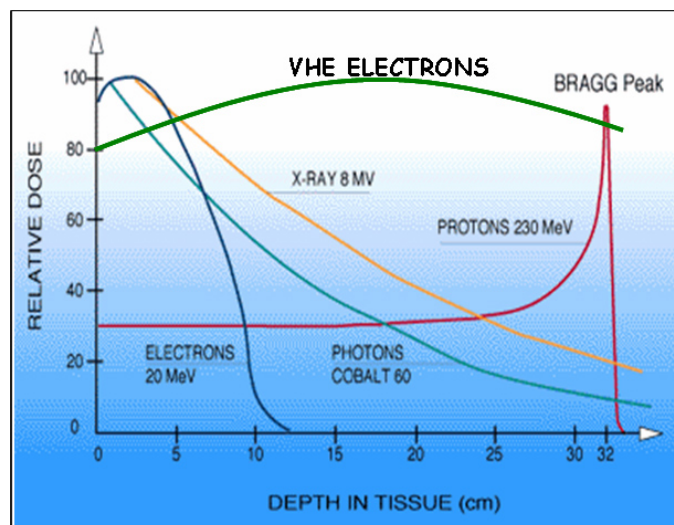

Figure 11 : Dose deposition for different particles

A detailed study of the dosimetric properties of monoenergetic VHE (very high energy) electron beams in the range of 150–250 MeV was published by DesRosiers et al.19 They have shown for instance that for parallel opposed beams the sharpness of the lateral penumbra is of comparable quality to that of clinical photon beams. The next step would be to evaluate the adequacy of VHE beams from laser-plasma interaction for IMRT. This requires a better knowledge of the dose deposition profile of a single electron bunch produced with present laser-plasma technology. Monte Carlo simulations with the code GEANT[15] were performed in order to show the dosimetric properties of the electron beam produced in the bubble regime. We assume that the low energy part of the spectrum can be removed. Since electrons are accelerated in a small region with dimensions comparable to the laser waist, we will use a pointlike electron source whose energy is distributed along a Gaussian shape with 40 MeV width FWHM, centered at 170 MeV[16]. The initial angular spread is chosen to be independent of the electron energy and corresponds to a Gaussian width of 10 mrad FWHM. A total of 10^5 electrons are used in the simulation. This value is lower than the measured number of electrons, which is about 3×10^9. This choice is a compromise between the time needed to complete the simulations and the statistical fluctuations. All output values are normalized with respect to the incident bunch charge. In order to obtain the dose for a single laser shot, one needs to multiply the normalized dose (in Gy/nC) by the charge of an electron bunch (0.5 nC). The following simulations are performed for a single shot, but our laser system can operate at 10 Hz. Fig. 12 show the contour plot of the dose deposited in water for a focused electron beam.
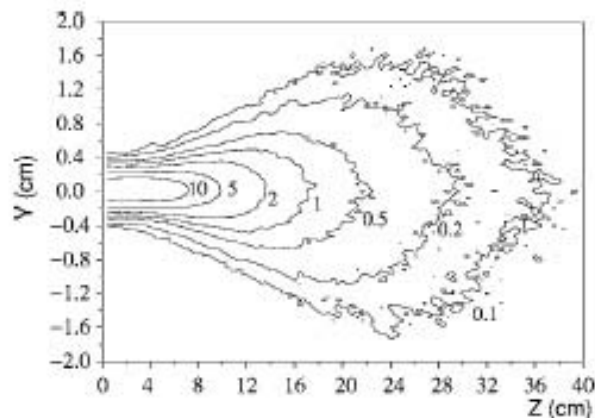

Figure 12 : Contour plot of the dose deposited inside water, for an electron beam focused at 30 cm in the water phantom with a 10 mrad divergence.

The dose distribution in water of a quasimonoenergetic electron beam with low divergence, produced by laser plasma interaction, reveals its interest for radiotherapy. Radially, the dose deposition profile is narrow and longitudinally, the penetration distance of these energetic electrons is higher than the 20 MeV conventional accelerators. The high laser energy conversion into accelerated electrons (10%) and the control of the interaction parameters may allow to obtain a tuneable electron source adapted to radiotherapy. Recent calculations done by DKFZ have shown that treatment planning quality in a prostate tumour can be improved by reducing the dose in safe tissue by 20%.

Applications to radiography

We have converted the electron beam from a laser-plasma accelerator into a γ -ray source using bremsstrahlung radiation in a dense material[17]. The γ-ray beam has a point-like

source size because it is generated by a high quality electron beam with a small source size and a low divergence. Using this γ -ray source, the radiography of complex and dense objects with sub-millimeter resolution has been performed. It was the first evidence of a γ -ray source size of a few hundreds micrometers with laser-driven accelerators. This size was consistent with results from Monte-Carlo simulations. Radiographies of complex objects were performed, compared to Monte-Carlo simulation results, and interpreted as indirect measurements of this small source size. It is a promising source for non-destructive material or mechanical inspection and it could also play an important role in clinical applications or in research fields where the size of the γ -ray source must be reduced. Images (calculated and measured) of dense object are presented in Figure 13. Analysis of these images indicated that the source size is smaller than 450 microns.
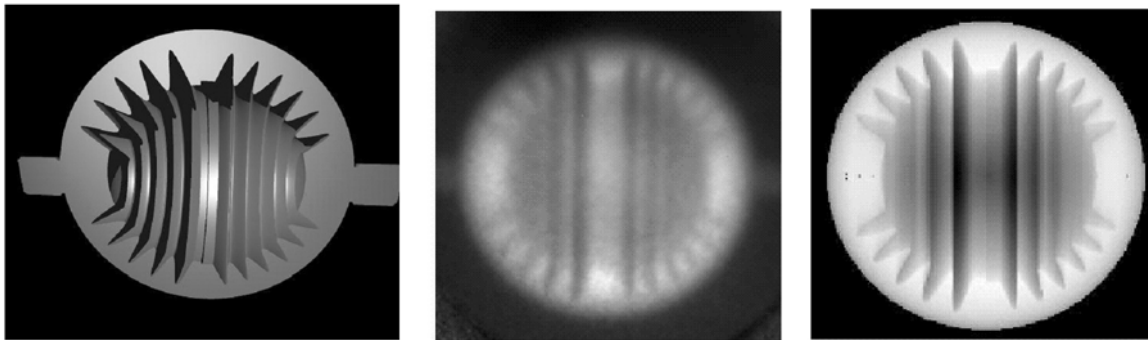

Figure 13 : γ radiography images (image of the object, experimental image and calculated image).

In addition to those studies we have demonstrated that the pulse duration is reduced its propagation in the underdense plasma, this relativistic compression will open new scheme to generate intense and very short laser pulse down to few optical cycle.

V. Multi GeV, low energy spread electron beam: Two stage accelerators design.

As shown in this report the bubble or the colliding laser pulses regime can produce electron beams at high energy with an energy spread of about 5 to 10 %. Numerical simulations show that with a 200 TW laser, electron energies of 1.5 GeV can be achieved in an homogenous plasma. Using a plasma channel, the laser power needed to reach similar gain is reduced to the 50 TW level. Nevertheless, since the energy transfer from the laser to the electron beam is the same, one has to find a compromise between the charge and the energy. The typical value for the laser to electrons energy transfer is of the order of 10 %. Assuming this value and a final electron energy of 1.5 GeV, for a 200 TW-50 fs laser (i.e 10 J) the charge will be limited to 666 pC, whereas for a 50TW-50fs (i.e 2.5 J), the maximum charge will be 166 pC.

In order to reduce the energy spread we propose here to inject the ultra short bunch of electrons we produced at LOA into a long plasma wave generated by a laser pulse in a low density plasma. We performed numerical simulations using the code WAKE. The laser is guided through a parabolic plasma channel with a radial density profile given by $n(r)=n_0$ $(1+0.585\ r/r_0\ )$, with $n_0 = 1.1\times10^{17}$ cm^{-3} and r_0 =47 μm and 24 cm long. The laser pulse duration is 60 fs, its energy, power and maximum intensity are respectively 9 J, 150 TW and 4.2×10^{18} $W.cm^{-2}$. The initial bunch mean energy is 170 MeV with an energy spread FWHM of 40 MeV, and its angular divergence is 10 mrad, The bunches are injected in the first wake with a radius of 8 μm. Figure 14 shows the energy spectrum of the extracted bunch. We can

see than roughly half of the electrons have been accelerated to 3.5 GeV, with a relative energy spread FWHM of 1% and an unnormalized emittance of 0.006 μm. The trapped fraction can be increased by reducing the initial bunch radius or by using wider pulses, which implies more laser energy.

Numerical simulations show that multi-GeV electron beams with low energy spreads can be produced in a very compact way by injecting electron beams produced today in the bubble regime into a long plasma wave structure. Importantly, the beam quality is preserved as well as its very short duration. On a longer time scale, developments of these novel beam acceleration techniques should also be of interest for high energy physics experiments.
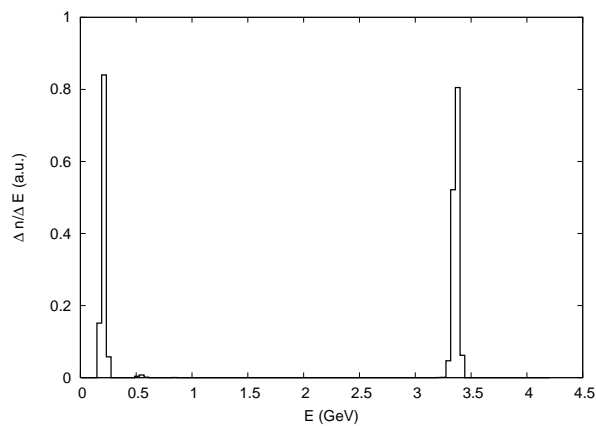

Figure 14: Final energy spectrum calculated for a guided laser pulse (60 fs, 9 J, 150 TW) and an acceleration length of 24 cm.

Acknowledgements

REFERENCES

1. Pukhov, A. & Meyer-ter-Vehn, J., Laser wake field acceleration: the highly non-linear broken-wave regime, *Appl. Phys. B* **74**, 355-361 (2002).

2. Malka, V. *et al.*, Monoenergetic electron beam optimisation in the bubble regime, *Phys. of Plasmas* **12**, 056702 (2005).

3. Mangles, S. *et al.*, Mono-energetic beams of relativistic electrons from intense laser plasma interactions, *Nature* **431**, 535 (2004).

4. Geddes, C. G. R. *et al.*, High-quality electron beams from a laser wakefield accelerator using plasma-channel guiding, *Nature* **431**, 538 (2004).

5. Faure, J. *et al.*, A laser-plasma accelerator producing monoenergetic electron beams, *Nature* **431**, 541 (2004).

6. Strickland, D. and Mourou, G., Compression of amplified chirped optical pulses, *Optics Comm.* **56**, 219 (1985).

7. Semushin, S. and Malka, V., High density gas jet design for laser target production, *Review of Scientific Instruments*, **72**, 7 (2001).

8. Glinec, Y. *et al.*, Absolute calibration for a broad range single shot spectrometer, *Review of Scientific Instruments*, **77**, 103301 (2006).

9. Faure, J. *et al.*, Ultra short laser pulses and ultrashort electron bunches generated in relativistic laser plasma interaction, *Phys. of Plasmas* **13**, 056706 (2006).

10. Glinec, Y. *et al.*, Observation of fine structures in laser driven electron beams using coherent transition radiation, *Phys. Rev. Lett.* **98**, 194801 (2007).

11. Esarey, E. *et al.*, Electron injection into plasma wake fields by colliding laser pulses, *Phys. Rev. Lett.* **79**, 2682-2685 (1997).

12. Faure, J. *et al.*, Controlled injection and acceleration of electrons in plasma wakefields by colliding laser pulses, *Nature* **444**, 737 (2006).

13. Lifschitz, A. F. *et al.*, Electron acceleration by colliding laser beams in plasmas http://arxiv.org/abs/physics/0703020

14. DesRosiers, C. *et al.*, 150–250 MeV electron beams in radiation therapy, *Phys. Med. Biol.* **45**, 1781 (2000).

15. Agostinelli, S. *et al.*, Geant4 -A simulation toolkit, *Nucl. Instrum. Methods, Phys. Res. A* **506**, 250 (2003).

16. Glinec, Y. *et al.*, Radiotherapy with laser-plasma accelerators: Monte Carlo simulation of dose deposited by an experimental quasimonoenergetic electron beam, *Med. Phys.* **33** (1), (2006).

17. Glinec, Y. *et al.*, High resolution γ-ray radiography produced by a laser-plasma driven electron source, *Phys. Rev. Lett.* **94**, 025003 (2005).

18. Malka, V. *et al.*, Staged concept of laser plasma acceleration toward multi GeV electron beams. *PRSTA* **9**, 091301 (2006).